

High energy hadrons in EAS at mountain altitude

[High energy hadrons in EAS]

J N Capdevielle[†], J Gawin[‡], D Sobczyńska[§], B Szabelska[‡],
J Szabelski[‡], and T Wibig[§]

[†] Laboratoire de Physique Corpusculaire, Collège de France, 11 place Marcelin Berthelot, 75231 Paris Cedex 05, France

[‡] The Andrzej Sołtan Institute for Nuclear Studies, 90-950 Łódź, Box 447, Poland

[§] University of Łódź, Experimental Physics Dept., ul. Pomorska 149/153, 90-236 Łódź, Poland

Abstract.

An extensive simulation has been carried out to estimate the physical interpretation of dynamical factors such as $\langle R_h \rangle$, $\langle E_h R_h \rangle$ in terms of high energy interaction features, concentrated in the present analysis on the average transverse momentum.

It appears that the large enhancement observed for $\langle E_h R_h \rangle$ versus primary energy, suggesting in earliest analysis a significant rise of $\langle p_t \rangle$ with energy, is only the result of the limited resolution of the detectors and remains in agreement with a wide range of models used in simulations.

Short title: High energy hadrons in EAS at mountain altitude

March 20, 2017

1. Introduction

Interest in the search for additional information in the hadron component of EAS at mountain altitude in terms of very high energy interactions [1] has been spurred by the necessity to have a continuity of multiproduction features between present colliders at $\sqrt{s} \leq 1.8$ TeV and the future LHC high energy physics at $\sqrt{s} = 16$ TeV (\sqrt{s} represents here the centre of mass energy for the nucleon–nucleon collision).

We review here the data obtained from calorimeters, or equivalent detectors, on high energy hadrons (longitudinal development and lateral spread) coupled with air shower arrays, where the primary energy is estimated from the electron and the muon components.

From qualitative considerations, the most energetic hadrons ($E_h > 1$ TeV) can be supposed to conserve some significant properties correlated with the dynamics of the earliest interactions: for instance, the relation between the transverse momentum p_t , the height h of the interaction, the hadron energy E_h and the radial distance R_h ,

$$p_t = \frac{R_h}{h} \frac{E_h}{c} \quad (1)$$

has been suggested as a possible measure of p_t [2].

Following this line of inquiry, special attention has been given to the measurements of quantities like $\langle E_h R_h \rangle$, $\langle E_h \rangle$, $\langle R_h \rangle$ (where $\langle \rangle$ are the mean values per hadron – see [3, 4]) and n_h , the number of hadrons above the energy threshold E_{th} . A convergent and significant increase of $\langle E_h R_h \rangle$ was observed in the different experiments [5, 6, 7] and the earliest interpretation was a tremendous rise of the transverse momentum $\langle p_t \rangle$, above $\sqrt{s} = 5000$ GeV, the minimum for p_t (occurring from equation 1 when the hadrons come directly from the first interaction) being situated around 2 GeV/c [2].

In more recent analysis measurements of hadron lateral distribution in Tien Shan calorimeter (which unfortunately have never been repeated [8]) have been interpreted in terms of increasing role of high p_t processes [9]. The problem still remains open, since the number of reports on the subject is small and “measurements of hadrons suffer more than other EAS components from systematic errors which have to be carefully estimated, using simulations of the detector response” [10].

In parallel with our review of the experimental data, we have carried out EAS simulations with the program CORSIKA version 4.50 [11, 12], regarded as containing the major features of the present collider physics, in the energy range $10^5 - 10^8$ GeV.

Our analysis has concentrated on the hadron lateral spread to explain the specific effects on the different factors combined in $\langle E_h R_h \rangle$, such as the sum of energy deposited, ΣE_h , the hadron distance, R_h , and the hadron content n_h (with consequences for the containment as well as the resolution of the detector). In order to appreciate the complexity of the hadron cascade mechanism, and how it can conserve or smear out the original interaction characteristics, the progression of our analysis is organized as follows:

- physical dependence of interaction parameters (multiplicity, inelasticity, p_t distribution....)
- dependence on primary spectrum and composition
- dependence on data acquisition and experimental resolution.

The survey of this dependence has focused on the largest detector employed, i.e. the Tien Shan calorimeter of 36 m² [5].

2. Simulation of the hadron lateral spread.

2.1. Assumptions on p_t and CORSIKA options.

The angular emission of secondary hadrons depends on the ratio $p_t/p_l \sim p_t/E_h$, where p_l is longitudinal momentum in laboratory system. Its evolution from CM frame to laboratory system is dominated, after Lorentz transformation, by the well known “collimation effect”, the emitted jet becoming narrower as the hadron energy increases. The multiplicity grows as $\ln^2 s$, inelasticity changes slowly and p_t rises regularly [11], but in reasonable proportion (circle shape points in figure 1).

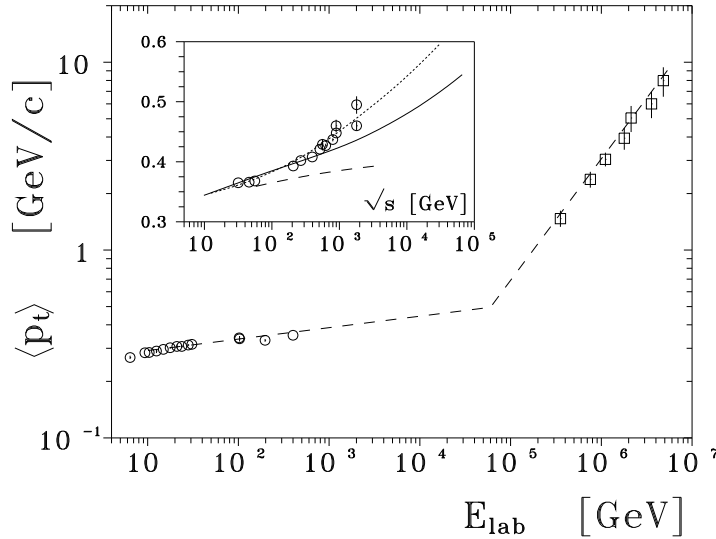


Figure 1. Dependence of $\langle p_t \rangle$ versus primary energy with the data interpretation of ref. [2] from $\langle E_h R_h \rangle$. In the window options in CORSIKA adapted from ref. [11]:

- 1. HDPM + CERN UA1 85 (solid line)
- 2. HDPM + CERN UA1 Mimi 96 (dotted line)
- 3. VENUS (dashed line).

○ accelerator and collider data compiled in [11]

□ $\langle E_h R_h \rangle$ interpretation from the Tien Shan experiment in [2].

Other effects, such as the increase in p_t for p–A collisions or A–A collisions (as described for the “Cronin effect” by Schmidt and Schukraft [13]), or correlated with jet production, or the increase in p_t for diffractive events [14] are not very important or can be disregarded according to their respective cross sections.

The correlation between $\langle p_t \rangle$ and multiplicity (or central rapidity density dn/dy) cannot be neglected in the treatment of individual events more correlated with the semi-inclusive data; the correlation of the UA1 experiment, described in [13], is included in CORSIKA package (for the option HDPM) and has been used,

without change, in the main part of our simulation. We have, nevertheless, performed some simulations with a p_t generator following the most recent correlation $\langle p_t \rangle$ with dn/dy from the CERN UA1 MIMI collaboration [15], characterized by a greater rise of $\langle p_t \rangle$ at large multiplicity. In this way, we ascertained that the subsequent relative changes in $\langle E_h R_h \rangle$ are of second order when compared to the attempt to explain $\langle E_h R_h \rangle$ with $\langle p_t \rangle$ values exceeding 2 GeV/c at $\sqrt{s} = 5$ TeV [2] (squares on figure 1).

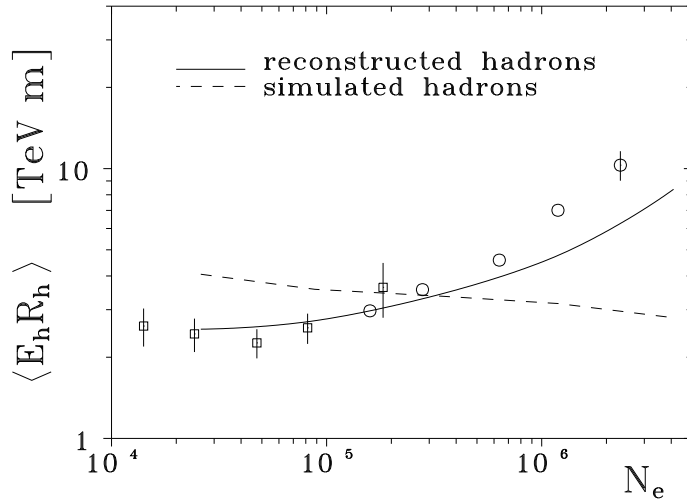


Figure 2. Dependence of $\langle E_h R_h \rangle$ versus N_e (for $E_{th} = 1$ TeV).
 – exact simulation (HDPM) output (dashed line)
 – after reconstruction described in section 3 (solid line)
 □ Tien Shan data [17]
 ○ Tien Shan data [18]

Furthermore some simulations have been done with this extremal value $\langle p_t \rangle = 2$ GeV/c around a primary energy $E_0 = 10^7$ GeV, after a special tuning of the p_t generator in CORSIKA: the options currently used have been HDPM in the usual form [12], as well as coupled to the p_t generator elaborated following UA1 MIMI results [19], and also the VENUS option [12]. A detailed description of the evolution with energy of the global interaction parameters used in the options of CORSIKA can be found in references [11] – [15].

The physical area explored following our selection of input parameters concerns primary energies between $10^5 - 10^8$ GeV, zenith angles between 0 and 30 deg for primary masses $A = 1, 4, 14, 28, 56$. The altitude for observation levels has been set to 3200 m with statistical samples of 500 simulated cascades per primary. Showers induced by heavy primaries have been simulated simultaneously with VENUS option and HDPM combined with superposition or, alternatively, with the abrasion-evaporation procedure [16], describing the fragmentation of heavy projectiles.

2.2. Consequences for the hadron lateral spread.

The results obtained for $\langle E_h R_h \rangle = (\Sigma E_h R_h)/n_h$ are shown in the figure 2 (dashed line), where $\langle E_h R_h \rangle$ is plotted versus electron size N_e , for proton primaries and for a hadron energy threshold $E_{th} = 1$ TeV. The expected decrease versus size, as in previous calculations [4], is obtained. The agreement is tolerable only for the experimental data [17] at N_e near $2 \cdot 10^5$. The lateral hadron densities Δ_h have been described by the experimenters with a simple exponential law:

$$\Delta_h = \frac{n_h}{2\pi R_0^2} \exp\left(-\frac{R_h}{R_0}\right). \quad (2)$$

We have used the same functional dependence to fit the hadron distribution in each individual shower with two free parameters: normalization related to the total number of hadrons n_h and mean radius R_0 . The total number of hadrons $\langle n_h \rangle$ varied from 0.05 for HDPM model and primary Fe to 0.9 for VENUS option and primary proton for $N_e = 10^5$ and respectively from 3.5 to 9.0 for $N_e = 10^6$. The average mean radius as a function of the shower size is presented in figure 3. Similar remarks as in figure 2 are suggested by figure 3, where R_0 decreases versus size, opposite to the general experimental tendency.

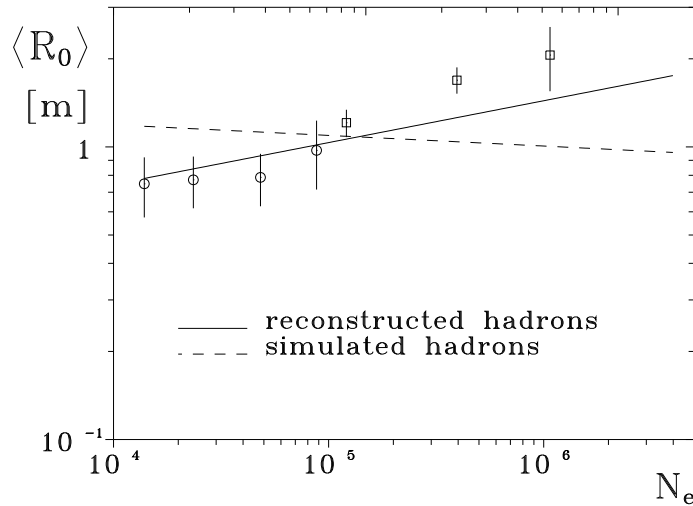


Figure 3. Dependence of $\langle R_0 \rangle$ versus N_e . (Lines and experimental data as in figure 2).

Table 1. Dependence of $\langle E_h R_h \rangle$ and $\langle R_0 \rangle$ on interaction and shower parameters from the simulations as noted.

Factors	A	$\langle E_h R_h \rangle$ (TeV m)	$\langle R_0 \rangle$ (m)	comment
a) primary mass A at $E_0 = 10^6$ GeV	1	3.16	1.6	HDPM +
	4	3.4	1.70	abrasion-
	14	3.67	2.21	evaporation [16]
	28	4.29	2.52	+ UA1 MIMI
	56	4.7	3.24	96 [15]
	56	3.81	1.34	HDPM+superp.
	1	3.73	1.09	Venus
	E_{th} (TeV)	$\langle E_h R_h \rangle$ (TeV m)	$\langle R_0 \rangle$ (m)	comment
b) hadron	0.32	1.988	1.24	HDPM
threshold energy E_{th}	1.0	3.34	1.01	
(primary protons	3.16	5.51	0.765	
of 10^6 GeV)	10.0	8.29	0.57	
	t_0 (gcm^{-2})	z	$\langle E_h R_h \rangle$ (TeV m)	$\langle R_0 \rangle$ (m)
c) initial conditions,	5	2	5.3	3.08
multiplicity	5	1/2	5.6	2.78
($z = n_{ch} / \langle n_{ch} \rangle$)	150	2	2.4	0.98
and depth (t_0) of first	150	1/2	2.5	1.26
interaction (primary		option:	HDPM	
protons of 10^6 GeV)				
	E_0 (GeV)	$\langle E_h R_h \rangle$ (TeV m)	$\langle R_0 \rangle$ (m)	option
d) primary energy	10^5	4.248	1.122	HDPM
(for protons	$3 \cdot 10^5$	3.678	1.08	
and for $E_{th} = 1$ TeV)	10^6	3.58	1.03	
	$3 \cdot 10^6$	3.34	1.01	
	10^7	3.00	0.95	
	10^8	2.69	0.93	

The total number of hadrons n_h reflects also a disagreement, characterized by an excess in the simulation [20], increasing with primary energy: the amplitude of this disagreement, when compared to the influence of primary energy and interaction parameters, is illustrated by the values calculated in table 1.

Setting $\langle p_t \rangle$ above 2 GeV/c around a primary energy $E_0 = 10^7$ GeV gave no rise in $\langle E_h R_h \rangle$ and $\langle R_0 \rangle$: a slight decrease was even observed due to the larger transverse mass per secondary and to the consequent enhancement of the inelasticity in the former collision, reducing in proportion ΣE_h at mountain level.

Table 1 represents a small part of the total simulation which contains similar effects to the examples presented. The total sample, up to 10^{17} eV, confirms general aspects of the dependence, that we can summarize as follows:

- $\langle R_0 \rangle$ and $\langle E_h R_h \rangle$ decrease with energy even if $\langle p_t \rangle$ is rising with energy.
- This effect persists even for extremal value of $\langle p_t \rangle = 2 \text{ GeV}/c$ and the “collimation effect” dominates over all the energy interval considered.
- The height of the first interaction has an effect on the lateral spread, increasing $\langle E_h R_h \rangle$.
- The factors $\langle R_0 \rangle$ and $\langle E_h R_h \rangle$ increase with the primary mass A .

3. Event topology and detector response.

The conditions of reception of the main hadron detectors employed at mountain altitude are compared in table 2.

Table 2. Hadron detectors at mountain altitude [5, 6, 7, 21, 22, 23].

Location	Detector	Area (m^2)	Energy range (TeV)	Resolution (cm)	Altitude (km a.s.l.)	Comment
Tien Shan	ionization calorimeter	36	≥ 0.3	25	3.2	axis contained
Chacaltaya I	em. chamber + burst det.	8		50	5.2	
Chacaltaya II	”	8	> 0.01	50	5.2	
Norikura	proportional counters + water tank + lead plates	25	0.02 - 0.12	50	2.77	$20m < r$ $r < 150m$

The hadron energy in the Tien Shan ionization calorimeter, composed of 850 g cm^{-2} lead, is measured at a depth between $130 - 850 \text{ g cm}^{-2}$ with an accuracy of 20% [24]. This thickness represents only $3.7 \Lambda_I$ (for an interaction length in lead $\Lambda_I = 194 \text{ g cm}^{-2}$) corresponding to a containment of about 80% of the cascades induced by individual hadrons [25]. The coordinates of the single hadrons are measured with an accuracy of 25 cm in the 744 ionization chambers of the calorimeter: those chambers, with an area of $(25 \times 300) \text{ cm}^2$, originally arranged in 15 rows, are intended to measure the hadron number with an accuracy of 5% [3]. Correction coefficients taking into account the limited lateral resolution and the possibility of aggregation of several hadrons within the chamber size bin $(0.25 \times 3) \text{ m}$ were introduced by Danilova [26] to recalculate the hadron energy spectra. The original method to separate and count the hadrons was based on the histograms of the ionization energy distribution in different rows in X and Y [18]. The limited efficiency of this treatment can be seen in figure 4, which shows real contained target diagrams for hadrons above 1 TeV and the same events reconstructed with the Tien Shan procedure; other difficulties appear also in the geometrical containment, the fraction of hadrons registered in one shower decreasing strongly with the primary energy (from 60% at $N_e = 10^5$ down to 20% at $N_e = 10^6$ according to our simulation).

The events simulated for section 2 have been treated by the numerical procedure of reconstruction of experimentally recorded detector response. The energy of each hadron was added to a respective ionization chamber output. As it is shown in

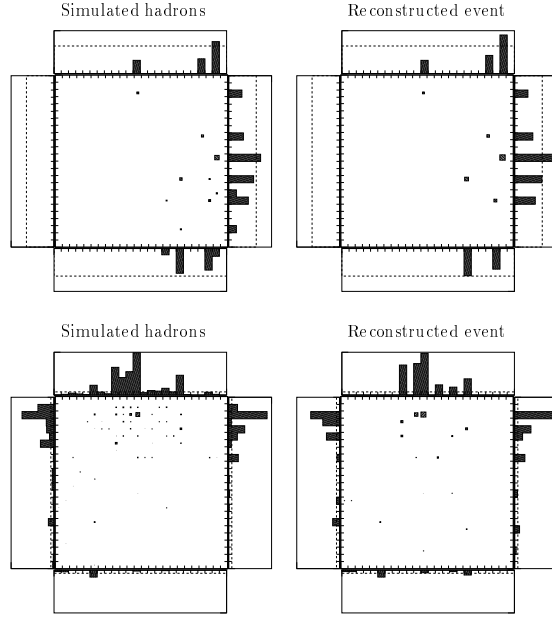


Figure 4. Two examples of total hadronic energy content of 10^6 and 10^7 GeV proton showers (upper and lower plots respectively) in each $25\text{ cm} \times 25\text{ cm}$ detector bin (and its four one-dimensional projections as side histograms) and the same after reconstruction procedure. Dashed lines in projection plots show the 1 TeV hadron energy threshold and the discrepancy can be due to the reduction factor (by 2.6) used in Tien Shan experiment in case of hadrons superposition [5, 18]. See text for more detailed explanations and comments.

figure 4 from a detector plane four one-dimensional projections are obtained (each chamber is 3m long while the detector size is $6\text{m} \times 6\text{m}$). Then on each projection the possible “hadronic cluster” coordinates have been determined. Using as a separation criterion the dip in the projected energy deposit distribution of at least 70% of neighbouring chamber outputs, close chamber signals could be combined just as it has been performed in the Tien Shan experiment. Then after comparing the amplitudes on respective x- and y-projections taking into account the possibility of overlapping of some hadrons in one of the projections the so-called “hadronic clusters” have been found. They will be called hereafter the reconstructed hadrons. They are shown in the right plots in figure 4.

Our reconstruction procedure includes also hadrons of energies below the threshold (1TeV) which are mostly added to the large hadronic clusters. The correction coefficient of 2.64 (equal exactly to the one used by the Tien Shan group) have been applied to the cluster energy while converted to the reconstructed hadron energy. The position of the reconstructed hadron was the energy weighted mean of chamber outputs in each projection. As the shower axis coordinates we have used the most energetic reconstructed hadron coordinates just like it has been done in Tien Shan experiment.

For all situations considered in section 2 the general decrease for $\langle E_h R_h \rangle$ and $\langle R_h \rangle$ vs size turns to a large increase (solid line in figure 2 and figure 3), as well as $\langle E_h R_h \rangle$ vs E_{th} (figure 5). This is confirmed (figure 6) by comparison with the most recent data [26] where the individual reconstruction indicates how the hadron content is underestimated near the axis. To preserve the clarity of the graphs, we have not

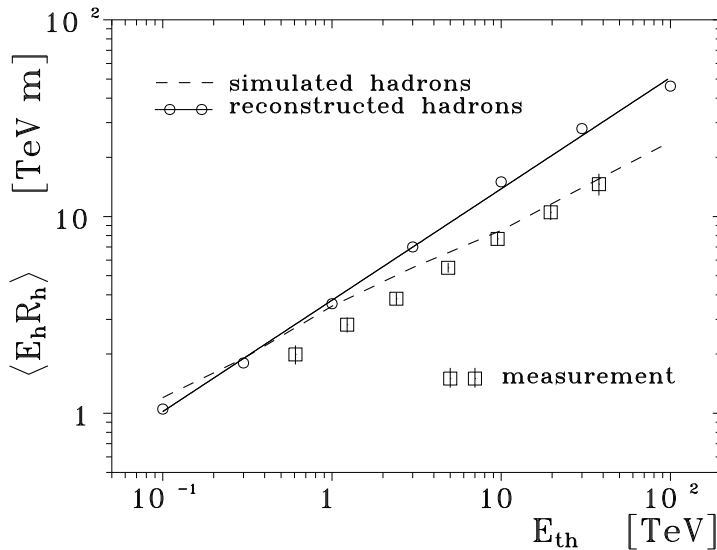


Figure 5. Dependence of $\langle E_h R_h \rangle$ on the energy threshold E_{th} . The squares are experimental points from [7] and [18]. The energy dependence of the simulation is parallel to the experimental behaviour.

plotted on figures 2 and 3 the results of the experiments [6], [7], [21] – [23] confirming the tendencies shown. Those values normalized to Tien Shan data can be found in reference [2] and reference [18].

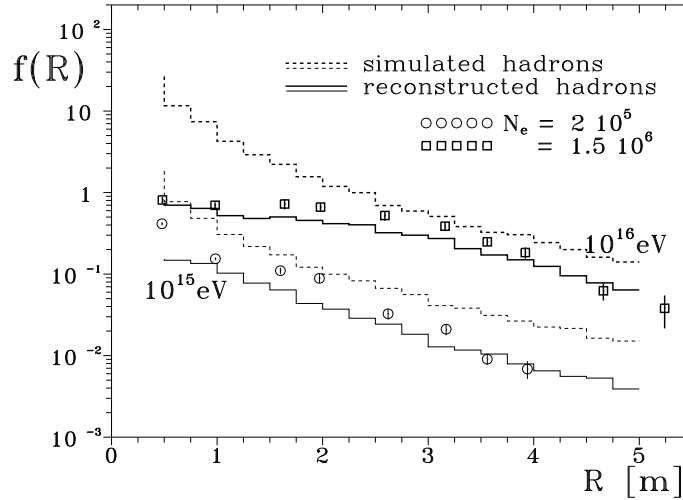


Figure 6. Hadron lateral distribution function $f(R) = dn_h/dR$ (for $E_h > 1TeV$) simulated and recalculated at 10^6 and 10^7 GeV. Experimental data [26].

4. Discussion

The proportion between the factor $\langle R_0 \rangle$ calculated in table 1 and the resolution distance quoted in table 2 shows the role of underestimation of hadron densities near the axis (when several hadrons enter simultaneously in the same chamber bin). This effect will be even greater than in the Tien Shan ionization calorimeter in all the other detectors quoted. The values of E_{th} correspond to larger hadron densities near the axis, increasing the probability of aggregation in the same chamber bin. Also for larger resolution distance (i.e. wider bins) this probability increases.

The simulation suggests that the hadron component and its lateral spread needs to be measured with more accurate calorimeters and a resolution distance substantially smaller than 25 cm.

We have shown that the rise $\langle E_h R_h \rangle$ is a consequence only of the complex treatment of the data which is inadequate for the superposition of hadrons, and the rise of $\langle p_t \rangle$ derived from $\langle E_h R_h \rangle$ and shown in the figure 1 is not valid. The lateral spread of muons above 200 and 500 GeV, also correlated with $\langle p_t \rangle$ in earliest interactions, doesn't require such an enhancement of $\langle p_t \rangle$ [27]; the main bulk of these lateral muon distributions being explained with a constant value of $\langle p_t \rangle = 0.4$ GeV/c [28].

As follows from our simulations, even if $\langle p_t \rangle$ is rising with energy, the hints in $\langle R_0 \rangle$ and $\langle E_h R_h \rangle$ cannot be expected to reflect the p_t behaviour, as they depend on several factors of the hadron cascade development.

To explain the enhancement in figure 2, an extremely large increase in primary mass, proportional to the primary energy, was introduced in the simulation [4] to transform the general decrease of $\langle E_h R_h \rangle$ versus N_e in a visible increase. Such conjectures are no longer necessary and the agreement can be obtained without a large increase of the primary mass.

The p_t dependence used here in the 3 options of CORSIKA covers a wide range of models; for instance, the values of p_t in option 2 are very close to the values used in SYBILL [29] as shown in [11] by Knapp, Heck and Schatz, and we can conclude that the present measurements of hadrons at mountain altitudes are in agreement with a majority of models used in EAS simulations. They require neither a large $\langle p_t \rangle$ enhancement nor a noticeable increase of primary mass. Their significance will remain limited until the resolution distance of the detectors is seriously improved. As it was advanced by Clay [30], “the results in hadron measurements depend critically on how well individual hadron signals are resolved in the hadron detector” and this has been confirmed by the present work.

Acknowledgments

This work has been done under the contract of collaboration between IN2P3 Paris and IPJ Warsaw and the authors are indebted to both institutions for their support. JS expresses his gratitude to N.M.Nesterova and V.A.Romakhin for very valuable discussions about experimental details of the Tien Shan hadron calorimeter.

References

- [1] Nikolsky S I 1998 *Proc. 15th ECRS (Perpignan)*, Nuclear Physics B (Proc. Suppl.) vol 60B p 144
- [2] Winn M M 1977 *Proc. 15th ICRC (Plovdiv)* vol 10 p 305
- [3] Romakhin V A, Nesterova N M, Dubovy A G 1977 *Proc. 15th ICRC (Plovdiv)* vol 8 p 107
- [4] Nesterova N M and Romakhin V A 1977 *Proc. 15th ICRC (Plovdiv)* vol 8 p 113
- [5] Aseikin V S et al. 1981 *prepr. no 178* (Lebedev inst., Acad. Nauk, Moscow) p 4.
- [6] Sreekantan S V, Tonwar S C and Viswanath P S 1983 *Phys. Rev. D* vol 28 p 1050
- [7] Böhm E and G.Holtrup G 1974 *Core structure of the hadron component in EAS, 4th ECRS (Lodz)* preprint
- [8] Nesterova N M and Romakhin V A 1998 *private communication*
- [9] Dubovy A G, Nesterova N M, Chubenko A P 1991 *Journal of Nuclear Physics* vol 54 p 178
- [10] Sivaprasad K 1996 *Il Nuovo Cimento* vol 19C no 5 p 643 (rapporteur talk given at the 24th ICRC, Rome, August 28 – Sept. 8, 1995)
- [11] Knapp J, Heck D and Schatz G 1997 *FK Report 5828*
- [12] Capdevielle J N et al. 1992 *The CORSIKA simulation program, KfK Report, (Karlsruhe)*
- [13] Schmidt H R and Schukraft J 1993 *J. Phys. G: Nucl. Part. Phys.* vol 19 p 1705
- [14] Goulianos K 1983 *Phys. Rep.* vol 101 p 169
- [15] Bocquet G et al. 1996 *Phys.Lett. B* vol 366 p 434 (UA1 - MIMI collaboration)
- [16] Attallah R, Capdevielle J N, Meynadier C, Szabelska B, Szabelski J 1996 *J. Phys. G: Nucl. Part. Phys.* vol 22 p 1497
- [17] Machavariani S K, Nesterova N M, Nikolsky S I, Romakhin V A, Turkish E I 1981 *Proc. 17th ICRC (Paris)* vol 6 p 193
- [18] Romakhin V A and Nesterova N M 1979 *Acad. nauk, Trudy ord. Len. Fiz. inst. Lebedev (Moscow)* vol 109 p 77
- [19] Capdevielle J N et al. 1997 *Proc. 9th IS VHECRI (Karlsruhe)*, Nuclear Phys. B vol 52B p 146

- [20] Dubovy A G and Nesterova N M 1983 *Proc. 18th ICRC (Bangalore)* vol 6 p 82
- [21] Miyake S, Ito N, Kawakami S, Hayashi Y, Awaji N 1979 *Proc. 16th ICRC (Kyoto)* vol 13 p 165
- [22] Matano T, Ohta K, Machida M, Kawasumi N, Tsushima I, Honda K, Hashimoto K, Aguirre C, Anda R, Navia C 1979 *Proc. 16th ICRC (Kyoto)* vol 13 p 185
- [23] Ticona R et al. 1993 *Proc. 23rd ICRC (Calgary)* vol 4 p 331
- [24] Nesterova N M and Dubovy A G 1979 *Proc. 16th ICRC (Kyoto)* vol 8 p 345
- [25] Bintinger D 1989 *Proc. workshop on calorimetry for supercollider (Tuscaloosa)* (ed. R. Donakson, World Scientific Teaneck N.J.) p 91
- [26] Danilova T V, Dubovy A G, Erlykin A D, Krutikova N P, Nesterova N M, Nikolsky S I, Yakovleva T I 1987 *Proc. 20th ICRC (Moscow)* vol 6 p 47
- [27] Vashkevitch V V et al. 1988 *Jad. Fiz.* vol 47 p 1054
- [28] Khrenov B A 1988 *Proc. 5th IS VHECRI, inv. and rapporteur papers* (University of Lodz Publishers) p 151
- [29] Gaisser T K et al. 1989 *Phys. Rev. Lett.* vol 62 p 1425
- [30] Clay R W 1985 *Proc. 19th ICRC (La Jolla)* vol 9 p 357 (rapporteur paper)